Acta Oceanol. Sin., 2024, Vol. 43, No. 1, P. 11–21
https://doi.org/10.1007/s13131-023-2268-5
http://www.aosocean.com
E-mail: ocean2@hyxb.org.cn

What induced the trend shift of mixed-layer depths in the Antarctic Circumpolar Current region in the mid-1980s?

Shan Liu[1]*, Jingzhi Su[2], Huijun Wang[3, 4], Cuijuan Sui[1]

[1] Key Laboratory of Marine Hazards Forecasting, National Marine Environmental Forecasting Center, Ministry of Natural Resources, Beijing 100081, China

[2] Center for Earth System Modeling and Prediction of CMA, Beijing 100081, China

[3] Collaborative Innovation Center on Forecast and Evaluation of Meteorological Disasters, Nanjing University of Information Science & Technology, Nanjing 210044, China

[4] Nansen-Zhu International Research Center, Institute of Atmospheric Physics, Chinese Academy of Sciences, Beijing 100029, China

Received 13 June 2023; accepted 10 October 2023

Abstract

An obvious trend shift in the annual mean and winter mixed layer depth (MLD) in the Antarctic Circumpolar Current (ACC) region was detected during the 1960–2021 period. Shallowing trends stopped in mid-1980s, followed by a period of weak trends. The MLD deepening trend difference between the two periods were mainly distributed in the western areas in the Drake Passage, the areas north to Victoria Land and Wilkes Land, and the central parts of the South Indian sector. The newly formed ocean current shear due to the meridional shift of the ACC flow axis between the two periods is the dominant driver for the MLD trends shift distributed in the western areas in the Drake Passage and the central parts of the South Indian sector. The saltier trends in the regions north to Victoria Land and Wilkes Land could be responsible for the strengthening mixing processes in this region.

Key words: mixed layer depth, trend shift, Antarctic Circumpolar Current (ACC), flow axis

Citation: Liu Shan, Su Jingzhi, Wang Huijun, Sui Cuijuan. 2024. What induced the trend shift of mixed-layer depths in the Antarctic Circumpolar Current region in the mid-1980s?. Acta Oceanologica Sinica, 43(1): 11–21, doi: 10.1007/s13131-023-2268-5

1 Introduction

The upper ocean mixed layer regulates air–sea exchange, including heat, freshwater, carbon and other important gases, which has widespread consequences for climate change and marine ecosystems (Deser et al., 1996; Ohno et al., 2009). The mixed layer depth (MLD) is a widely used variable in the upper ocean to quantitatively depict the mixed layer (Giunta and Ward, 2022), which delimits the quasi-homogeneous region of the ocean with active turbulence.

Many studies have focused on MLD variability on regional and global scales. For example, An et al. (2012) analyzed the MLD seasonal variation over the global ocean using gridded Argo data and noted that unlike the situation in the North Pacific and North Atlantic, the MLD in the North Indian Ocean is mainly influenced by strong monsoons there. Sallée et al. (2021) assessed the multidecadal evolution of the mixed layer and pycnocline across the world ocean and found that summertime density contrast increased at a higher speed than previous estimates and that the summer mixed layer deepened. In addition, due to the importance of the MLD, the representation skills of the mixed layer in climate models have been assessed for the Coupled Model Intercomparison Project Phase 3 (CMIP3), CMIP5 and CMIP6. A common problem is that the simulations in summer season are consistently shallower than those in observations (Downes et al., 2009, 2010; Sallée et al., 2013; Huang et al., 2014; Zhang et al., 2018; Liu et al., 2023).

Among the sensitive regions where the MLD has large variability on seasonal to decadal time scales, the Antarctic Circumpolar Current (ACC) is prominent. The strength of the ACC is believed to be closely associated with the westerly wind stress blowing over the Southern Ocean, which has experienced pronounced subsurface warming, widespread freshening and increasing anthropogenic carbon over the past several decades. Moreover, the ACC has been confirmed to accelerate in the context of global warming (Shi et al., 2021). As these eastward currents are the primary agents through which oceanographic properties such as heat, salt and dissolved chemicals are transferred between ocean basins (Stewart, 2021), ocean dynamic and thermal conditions are bound to be affected in the future. It is generally acknowledged that the upper ocean tends to become warmer and density stratification tends to strengthen in a warming world. However, ocean MLD variability shows many uncertainties (Sallée et al., 2021). Moreover, compared with the mechanism associated with surface stratification (Li et al., 2020; Yamaguchi and Suga, 2019), the reasons leading to MLD variations are more complicated and harder to explain. Previous studies have mainly focused on the overall linear trend of MLD on a global scale (e.g., Somavilla et al., 2017; Sallée et al., 2010, 2021) but have not specifically explored the MLD trend variation and its attribution analysis in the ACC region. However, this study noted that the MLD trend in the ACC region underwent a decadal shift around the mid-1980s. Before and after the decadal transition, the MLD variation trend in the ACC region is apparently different. What induced the trend discrepancy between the

Foundation item: The National Natural Science Foundation of China under contract No. 41605052.
*Corresponding author, E-mail: liu_shan_@126.com

two stages?

The present study reveals that there is a trend shift in the MLD variation in the ACC region and studies the possible drivers. The rest of this article is organized as follows. The data and methods are described in Section 2. The MLD trend shift in the ACC region and the contributing factors are analyzed in Section 3. A summary and discussion are given in Section 4.

2 Data and methods

2.1 *Data*

The Institute of Atmospheric Physics (IAP) monthly global ocean temperature and salinity product (Cheng et al., 2017) at a 1°×1° horizontal resolution with 41 levels in 0–2 000 m for 1960–2021 is used to calculate the MLD and investigate its linear trends. The temperature at the surface level (1 m) is used as the sea surface temperature (SST). The ECMWF Ocean Reanalysis 5 (ORA5) dataset of monthly current velocities on a 0.25°×0.25° grid during 1960–2021 is employed to check the variation in ocean surface current. They are regridded onto the grid of 1°×1° to facilitate the comparison. To analyze the flux exchange between the ocean and atmosphere on the surface, the European Centre for Medium-range Weather Forecast (ECMWF) fifth generation atmospheric reanalysis (EAR5; Hersbach et al., 2020) monthly averaged data from 1960–2021 are used, including 10 m wind speed, 10 m horizontal wind, mean total precipitation rate, mean evaporation rate, mean surface net shortwave radiation flux, mean surface net longwave radiation flux, mean surface latent heat flux and mean surface sensible flux with a resolution of 1°×1°.

2.2 *Methods*

The MLD is computed based on the monthly mean temperature and salinity. The MLD is defined as the depth at which the potential density referenced to the surface exceeds the density of the water at 10 m by a threshold of 0.03 kg/m^3. This criterion has been shown to robustly detect the depth of the mixed layer in various regions of the ocean (de Boyer Montégut et al., 2004; Sallée et al., 2021).

The linear long-term trend in each grid cell is calculated from the MLD anomalies using a least-squares fit. Student's t test is used to examine the significance for variable trends.

To clarify the position variations of the ACC, the flow axis is analyzed. The ocean current axis is meridional meander where the maximum current velocity occurs, roughly a latitude circle around the Antarctic continent. In addition, the circle of maximum wind speed near the ocean surface can also reflect the change of the flow axis. Moreover, there are obvious reverse shear vortices on both flanks of the maximum wind speed line, so the meridional gradient of wind stress curl could also be a representation for the flow axis position. Therefore, the above three proxies are all selected to analyze the position variation of the flow axis for mutual verification. More specifically, the circumpolar contours for the maximum of wind speed, current speed and meridional gradient of wind stress vorticity from 40°S to 65°S are calculated to represent the climatic mean core position of the ACC. For moving tendency, all positive trends on each longitude from 40°S to 65°S are normalized to obtain the weight coefficients first, and the trends circumpolar of the ACC flow axis is represented by the corresponding weighted averaged position contour.

3 Results

3.1 *The long-term trend for MLD in the ACC region*

The annual mean and seasonal MLD time series in the ACC region are displayed in Fig. 1. The time evolution of the MLD exhibits pronounced interannual and decadal variabilities (Figs 1a, c and e). An obvious trend shift of the MLD can be found, with a period with decreasing trend and then a period with almost no trends. The transition between these two time periods occurred around the period from the 1970s to mid-1980s.

To determine the turnaround year of the trend shift more accurately, a quantitative analysis was conducted using the annual mean result. The cutoff point was tested by each year within the period during 1970 to 1985, and then the trend between 1960 and that cutoff year were calculated and evaluated. Results indicate that when cutoff year moves to 1985, the downward trend of the MLD is –0.18 m/a, and this trend exceeds the 99% confidence level for the first time. While in the subsequent period after 1985, the trend is quite weak, with a value of –0.005 m/a.

The MLD trends in austral winter (August–October) and summer (January–March) exhibit different patterns (Figs 1c, e). In austral winter, there is a shallowing trend followed by a weak variation in the later period, which is similar to the annual mean result. On the other hand, the MLD trend in austral summer shows an upward trend of 0.03 m/a in the second phase, which is inconsistent with that in austral winter. The magnitude of MLD variation is much greater in winter than that in summer. The climatic mean MLD in ACC region are around 63.7 m, 18.9 m and 38.3 m for winter, summer and annual mean results, respectively. Moreover, the annual mean MLD variation is almost entirely dominated by the temporal changes of the austral winter MLD, and the time correlation coefficient between them is as high as 0.91.

The variation of SST is gentler than MLD. The climatic mean SST in ACC region are around 4.5℃, 6.5℃ and 5.4℃ for winter, summer and annual mean results. Unlike the MLD trend in the ACC region, SST variation maintained an upward trend whether before or after the mid-1980s (Figs 1b, d and f). The trend difference of SST between the two periods is not significant. For the annual mean result, the SST trends in the two periods are 0.01℃/a and 0.006℃/a. While for the austral winter (summer) results, the trends are 0.009℃/a (0.01℃/a) and 0.005℃/a (0.007℃/a), respectively.

In principle, mixed-layer shoaling on a large spatial scale is well understood under a global warming background due to intensified stratification (Sallée et al., 2021). However, the unexpected MLD trend in the ACC region is more complex, which needs more investigation. Due to the dominating role of winter MLD for the annual mean results, the following analyses are focused on the annual mean and winter MLD, as well as the contributing factors in both two periods.

3.2 *The spatial pattern for MLD trends in the ACC region*

Since MLD showed different trends before and after the mid-1980s, the spatial patterns of the MLD trend are analyzed in the following two periods: 1960–1985 and 1986–2021. Figures 2a–c show the magnitudes of spatial long-term linear annual mean MLD changes for the ACC region during the above two periods and their differences, with field mean of –0.180 m/a, –0.002 m/a and 0.178 m/a. In the former period, the MLD was shallowing in almost all area of the ACC region, except for the areas south to Australia and in areas of the central Pacific (45°–60°S, 180°–120°W). The maximum shallowing trend is –8.22 m/a around the area off the northernmost point of the Antarctic Peninsula. In the latter period, the shallowing trend almost diminished and deepening MLD emerged in the ACC region (Fig. 2b). The maximum deepening rate in the ACC region is 2.37 m/a around in the area

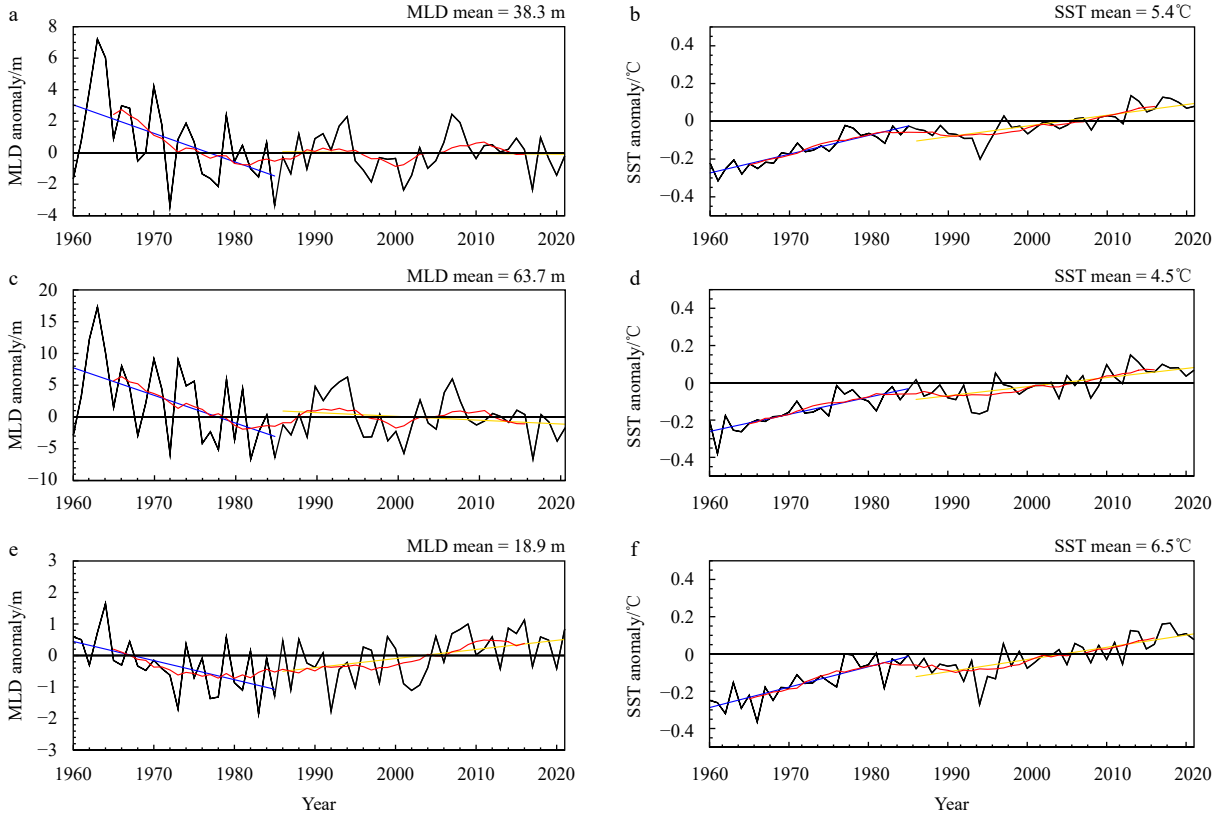

Fig. 1. Annual mean MLD (unit: m) (a) and SST (unit: ℃) (b) anomaly time series in the ACC region (35°–65°S) for the period of 1960–2021 (taking 1991 to 2020 as the climatology). The blue and yellow lines are the linear trends for the periods of 1960–1985 and 1986–2021, and the red lines are the 11-year running mean of the corresponding black lines. The long-term mean (1960–2021) values are shown in the right up corners. (c, d) and (e, f) are the same as (a, b), but for austral winter (August–October) and summer (January–March) respectively.

north to the Wilkes Land. The annual mean MLD climatology during the two periods differs little from each other, with a eastward shift for the MLD high value centers (about 150 m) both in South Indian (SI) and South Pacific (SP) sectors. Figure 2c demonstrates that the MLD trends sharply shifted around the mid-1980s, with the most concentrated positive trend differences distributed in the western area in the Drake Passage, the areas south to Australia, and the mid-latitudes in the central parts of the South Indian Ocean (SIO). The maximum deepening trends corresponding to the above centers are 5.86 m/a, 6.49 m/a and 5.65 m/a, respectively. The SST patterns are displayed in Figs 2d–f, and the trend field mean for the two periods and their difference are 0.010℃/a, 0.006℃/a and –0.004℃/a, respectively. During the period of 1960–1985, strong warming trends occupied most areas in the ACC region, with high values concentrated in the central SIO (35°–50°S, 60°–120°E). However, these warming trends decayed, and scattered cooling trends appeared in the Subantarctic region from 1986 to 2021. The trend shift of SST shown in Fig. 2f mainly demonstrates three relatively-weakening warming centers, which corresponds well with the deepening trend centers of MLD in Fig. 2c.

Winter mean MLD and SST trend patterns are shown in Figs 2g–l. The variation patterns of winter MLD in both two periods are quite similar to the annual mean results, but with significantly stronger magnitudes. The climatic MLD peak values are about 300 m, almost twice that of annual mean results. The trend field mean of the two periods and trend shift are of –0.408 m/a, –0.081 m/a and 0.327 m/a. In the three key regions mentioned earlier, the positive winter MLD trends reach 14.83 m/a, 13.31 m/a and 16.56 m/a, respectively. The spatial distribution of winter SST trend patterns also closely resembles the annual mean SST trend patterns. However, unlike the increased amplitudes in winter MLD, the magnitudes variations of SST and its trends between the winter and annual mean results are relatively small. The SST trend field mean in winter are 0.009℃/a, 0.005℃/a and –0.004℃/a, almost same as the corresponding annual mean value. In the three relatively-weakening warming regions, the SST trends difference in winter exhibit extreme values of –0.07℃/a, –0.07℃/a and –0.12℃/a, respectively.

3.3 *Contributing factors controlling the MLD trend shift*

Cause analysis of the evolution mechanism of the MLD trend shift in the ACC region was carried out here to explore the possible drivers, by analyzing wind speed, ocean current, wind stress vorticity, net heat flux and freshwater flux.

The MLD variability may be affected by the wind field. Wind stirring can generate mechanical mixing, wave breaking, internal waves and other submesoscale instabilities in the ocean mixed layer, which can contribute to vertical convection (Huang et al., 2012; Barkan et al., 2017; Buckingham et al., 2019). Moreover, vertical mixing could also be affected by the ocean current and wind stress vorticity, which are both closely associated with winds through Ekman pumping and Ekman transport (Huang and Qiu, 1998).

Figure 3 displays the corresponding trends for the wind field, ocean current and wind stress vorticity. The ACC region is dom-

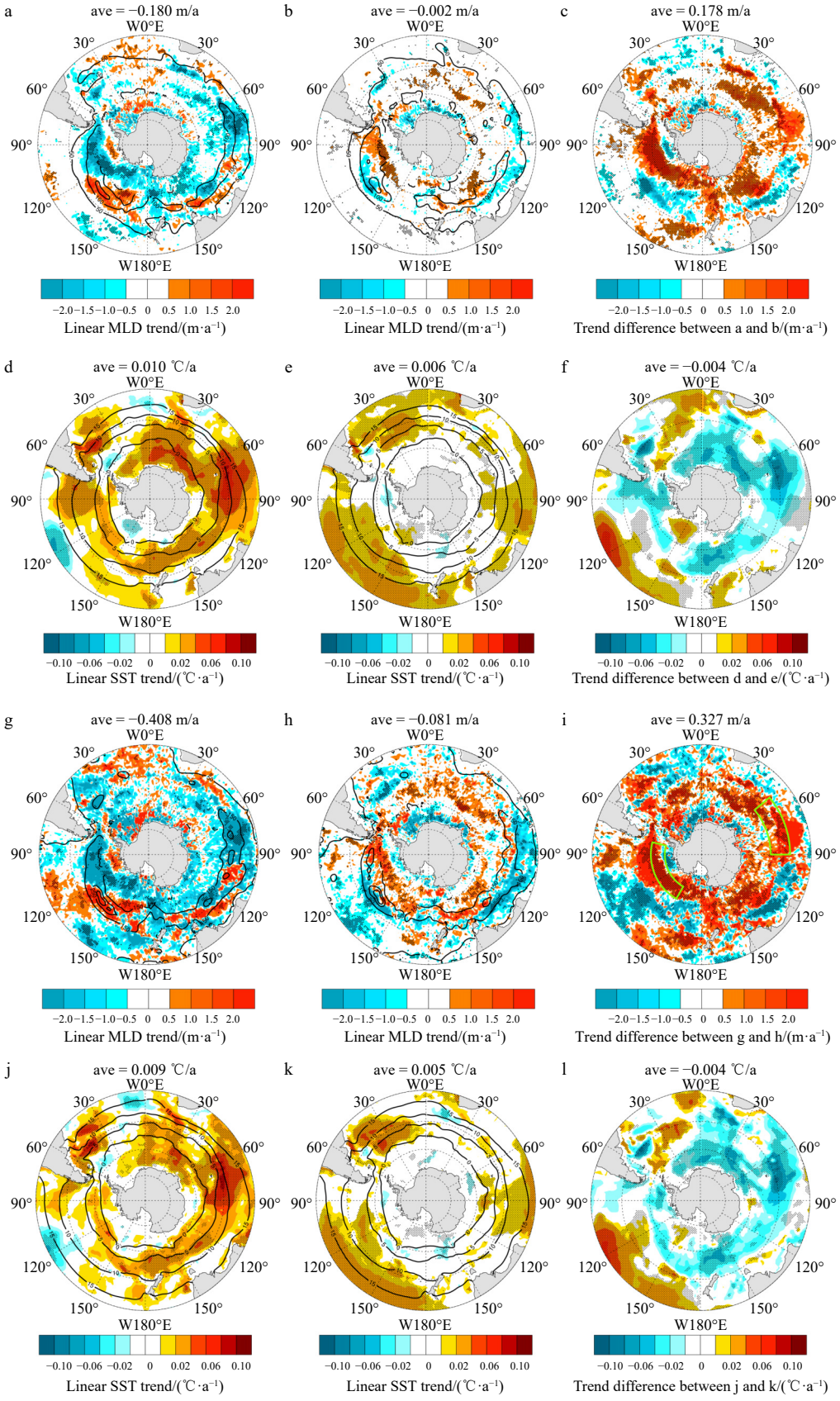

Fig. 2. Spatial patterns of the linear MLD trend (shaded areas) and the MLD long-term mean (black contours) for periods 1960–1985 (a) and 1986–2021 (b). c is the trend difference between a and b. d–f are the same as a–c, but for SST and its trends. g–i and j–l are the spatial patterns of MLD and SST in austral winter. The "ave" values are their respective trend mean. The dotted areas exceed the 95% confidence level.

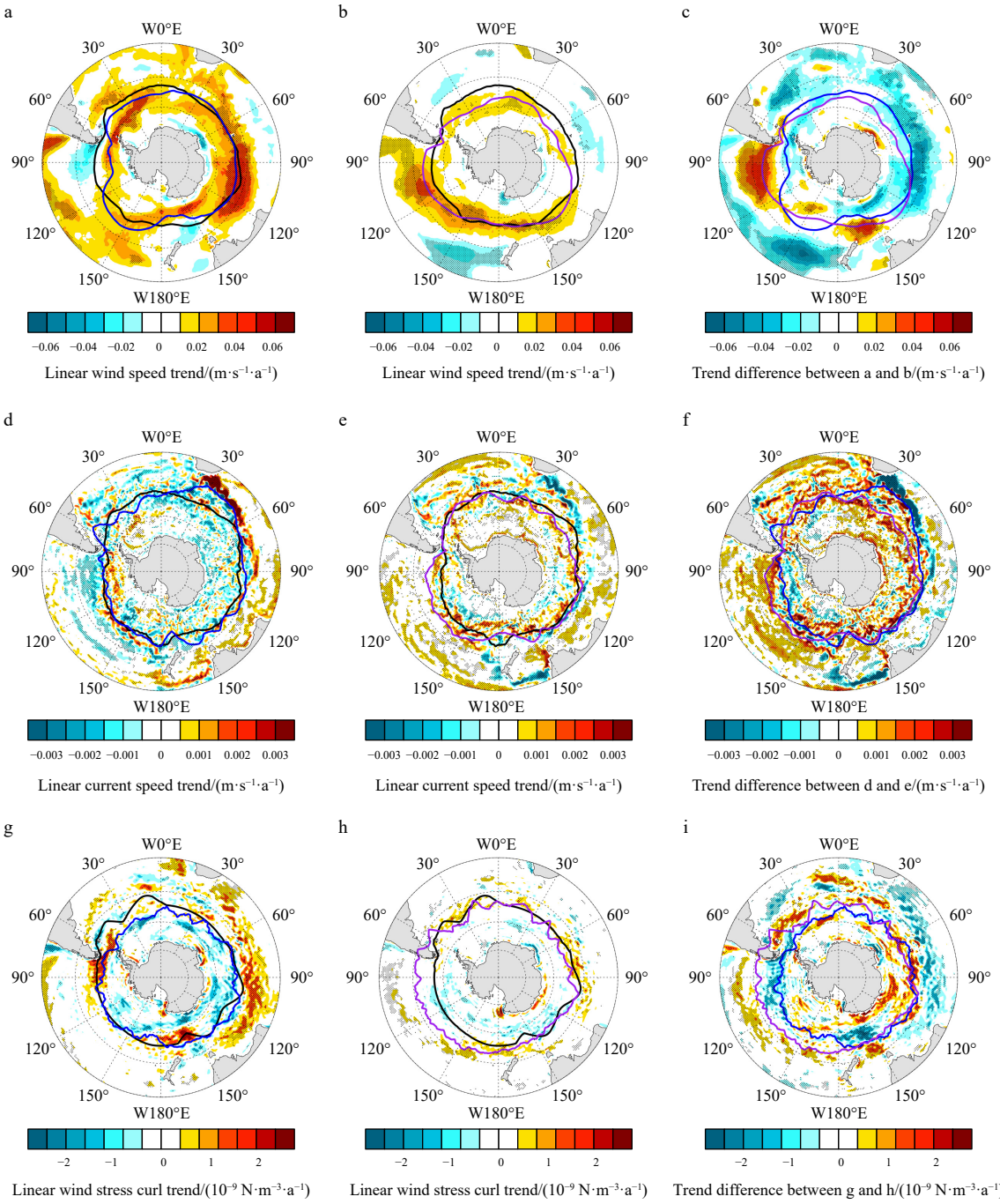

Fig. 3. Spatial patterns of the linear wind speed trend in the ACC region for 1960–1985 (a) and 1986–2021 (b). c is the difference between a and b. d–f and g–i are the same as a–c but for surface ocean current speed and wind stress curl. The black contours in a and b are the climatic core position of the ACC (1991–2020). The blue and purple contours in a–c are the trends circumpolar contours for period 1960–1985 (a) and 1986–2021 (b). The contours in d–f and g–i are the same as a–c but for ocean current and wind stress vorticity.

inated by intense westerly winds almost all year round. Many studies have focused on the association between wind momentum and physical processes in the upper ocean (e.g., Russell et al., 2006; Toggweiler and Russell, 2008; Feng et al., 2020). The wind speed during 1960–1985 showed a significant intensification trend in almost all area of the Southern Ocean, and the strongest trend reached as high as 0.053 m/(s·a). However, after the mid-1980s, the strengthening winds mainly shrank to the Pacific sector and the Indian sector. Although the wind speed in the ACC region increased throughout the period after 1960 (Yang et al., 2007; Liu and Wu, 2012), the trend in the later period was significantly weaker, especially in the South Atlantic (SA) and SI sector, which can be well reflected in the trend difference shown in Fig. 3c. The strongest value of the wind speed reduction rate was –0.054 m/(s·a) in the central SI region.

The trends of surface ocean currents are quite different from the wind fields mentioned above (Figs 3d–f). In the former period, the weakening trends of surface ocean currents occupied

most regions, while in the latter period, negative trends decayed, and positive trends appeared in more areas. Therefore, the dominant trend shifts for surface ocean currents are positive, especially in the SP sector (Fig. 3f). The trends of surface ocean currents do not keep pace with those of winds, which is consistent with the conclusion that the ACC resists wind-driven acceleration in both observations and model simulations (Munday et al., 2013; Böning et al., 2008).

The wind stress curl trends are displayed in Figs 3g–i. In the ACC region, the trends of the wind stress curl are distributed surrounding Antarctica, roughly along the flanks of the ACC. In both periods, negative values of wind stress vorticity trends were located closer to Antarctica, while the positive values expanded equatorward in all ocean sectors. The differences in wind stress curl trends (Fig. 3i) show trend differences with maximum and minimum trends of 6.4×10^{-9} N/(m^3·a) and -11.9×10^{-9} N/(m^3·a) respectively.

To further explore the possible influence of dynamic fields on the MLD trend shift, the flow axis of the ACC is analyzed. The maximum wind speed circumpolar contour in 40°–65°S is selected to be a proxy for the climatic mean position of the ACC. In addition, the weighted average position of the positive trends on each longitude is chosen here to represent the moving trend for the maximum wind speed circle (Figs 3a–c). The meridional location of surface wind did have an interdecadal shift in the two periods, especially in the SI and SP sectors. Moreover, this shift is not symmetrical and does not contract at all longitudes, but it shows a polarward shrinking trend in SI and an equatorial expansion trend in SP. That is, the center of the maximum wind speed circle tends to move toward the Marie Byrd Land direction. The locations of surface ocean current speed (Figs 3d–f) are quite similar to those derived from trends of wind speed. In the analysis of the wind stress curl, the maximum meridional gradient of the wind stress curl trend is used to compare the core meanders of the ACC. In general, there are opposite vorticities on the southern and northern flanks in the ACC region. Therefore, it can be deduced that the location with the maximum meridional gradient of vorticity is just the place where the flow axis exits. Consistent with previous conclusions derived from wind speed and current, the circumpolar contour of the maximum meridional gradient of wind stress vorticity also exhibits a concurrent shift toward the Marie Byrd Land direction.

Figure 4 depicts the winter trend spatial patterns of wind speed, ocean current, and wind stress vorticity. The spatial trend patterns of wind speed in winter are generally similar to the annual mean results (Figs 3a–c). The main differences are as follows. In the former period, the increasing trend of wind speed over the area southeast to New Zealand shifted to a decreasing trend; in the latter period, the increasing trend of wind speed in this region became more significant, which led to a severe trend shift between the two phases during winter (Fig. 4c). There is a band-like area (43°–52°S, 180°–70°W) with wind speed increasing trend with a mean amplitude of 0.06 m/(s·a). Negative trend shift is also evident in the SA and SI regions. Regarding the maximum wind speed axis, there was a notable moving tendency towards the SP sector direction in the second phase, exhibiting a greater fluctuation compared to the annual mean results (Fig. 3c). The trend variations of surface ocean current are highly stable, with little difference in intensity and spatial distribution between winter and the annual mean results. The changes of the flow axis align with the movement of the annual mean as well (Figs 4d–f). Comparing the trend distribution of wind stress curl during winter with the annual mean results, the patterns are similar, but the magnitudes in winter are significantly stronger in all ocean basins. The most significant changes of winter trends for wind stress curl occurred in the SP sector in both two periods. For the position of the flow axis, although the vorticity trends on both flanks all increase, the position of the maximum curl gradient shows little change, exhibiting a shift to low latitudes in the SP sector (Figs 4g–i). In general, the trend patterns of dynamic variables in winter are consistent with the annual mean results, but with larger variations which primarily occurs in the SP sector.

Figure 5 displays the zonal mean profiles of wind speed, ocean current, wind stress vorticity and MLD in the two periods in both the SP (40°–65°S, 180°–70°W) and SI (40°–65°S, 0°–90°E) sectors. The solid and dashed lines represent the annual mean and winter results respectively. In the SP sector (Figs 5a–d), the annual (winter) mean climatological zonal mean wind speed peaks at approximately 55°S (58°S). From 1960 to 1985, the wind speed increasing trend was most obvious in the region south of 60°S. From 1986 to 2021, the annual (winter) mean strengthening trends of wind speed reached their apex at approximately 51°S (47°S), which apparently resulted in a shift toward the equatorial direction for the wind speed extreme. In terms of ocean currents, the annual mean and winter results have little difference. There was a slight accelerating trend in the region south of 60°S in the former period, and the positive trends moved to latitudes between 45°S and 55°S in the latter period, indicating an equatorial migration. Moreover, the positive to negative transitions of wind stress vorticity also support the same result. The climatological transition of annual mean (winter) wind stress vorticity occurs at 52°S (56°S). The sign of wind stress vorticity trends changed from positive to negative at approximately 60°S during the former period. However, this change arose at lower latitudes of approximately 52°S for annual mean results and 48°S for winter mean in the subsequent period. All these variations indicate that the ACC meanders in the SP sector have shifted toward the equator.

The mitigation in the SI sector is different from that in the SP sector (Figs 5e–h). The climatological zonal mean wind peak is located at approximately 50°S in the SI sector, and the accelerating trend maximum of wind shifts from 52°S to 54°S for annual mean results (54°S to 59°S for winter mean), manifesting a slight polarward shift. In terms of ocean currents, the climatic peak value appeared at 48°S, and there was a slight weakening trend along almost all latitudes from 1960 to 1985. However, strengthening trends replaced the weakening trends south of 46°S from 1986 to 2021, which displayed a poleward mitigation trend for the maximum current contour. Analyzing from the turning point of the wind stress vorticity from positive to negative, the climatological transition is shown at approximately 50°S. In the first period, the transition occurred at 50°S for annual mean result (53°S for winter mean). However, the watershed moved significantly southward to higher latitudes of approximately 54°S (61°S for winter mean) in the second period. The zonal mean profiles of wind speed, ocean current and wind stress curl all indicated a polar shift of the meridional meanders of the ACC in the SI sector.

Taken together and further confirmed by the conclusions drawn in Figs 3 and 4, there was a drift in the flow axis of the ACC, as well as the wind speed and wind stress vorticity field. The SP sector experienced expansion in the equatorial direction, while the SI sector experienced polarward compression in the meridional direction. The center for the axis of the entire circumpolar currents moved toward the Marie Byrd Land direction of the Antarctic.

Up to this point, it is determined that although the trend distributions in the three dynamic fields have their own characteristics, a significant commonality is shared by all of them, which is

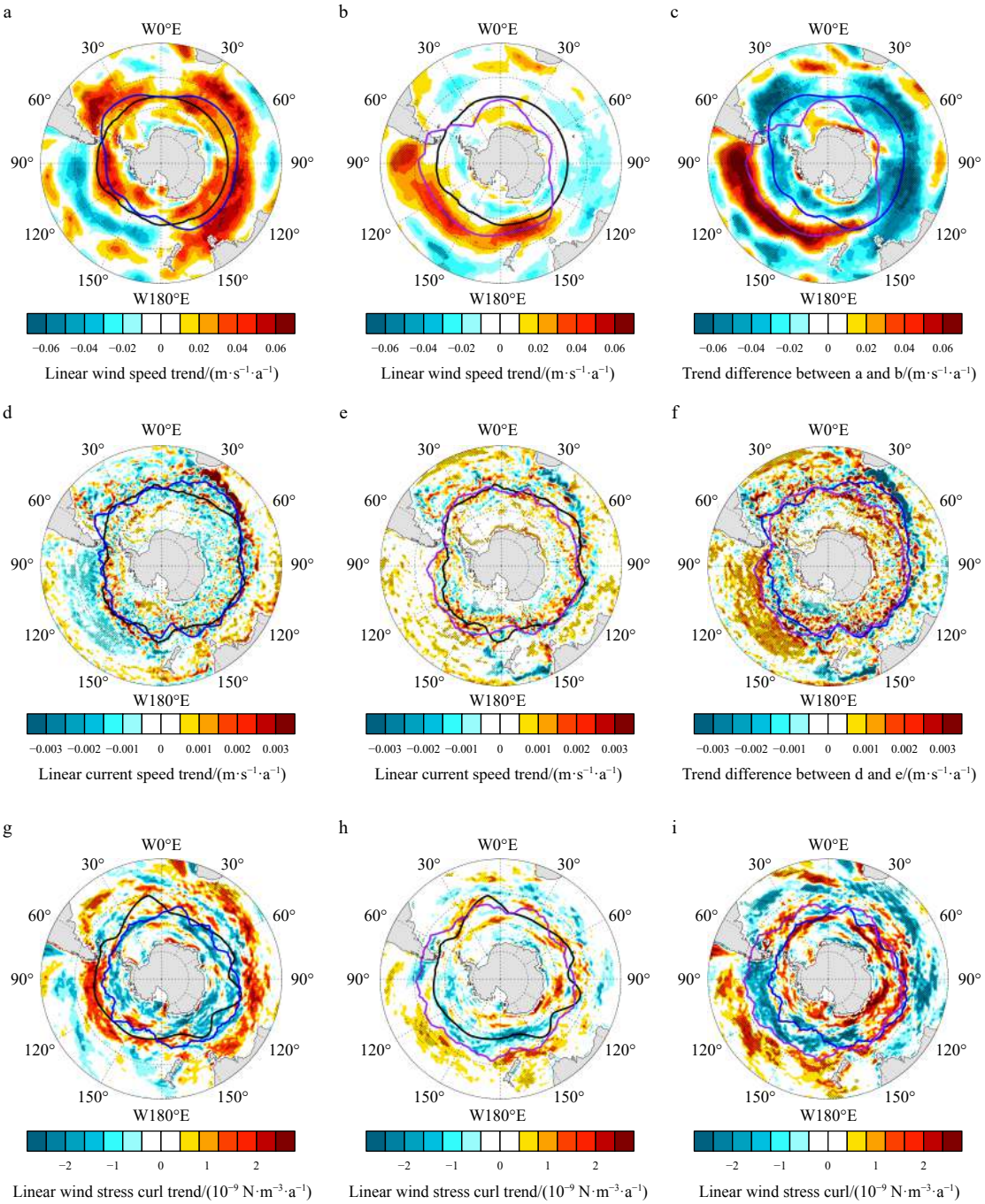

Fig. 4. Spatial patterns of the linear wind speed trend in the ACC region for austral winter in 1960–1985 (a) and 1986–2021 (b). c is the difference between a and b. d–f and g–i are the same as a–c but for surface ocean current speed and wind stress curl. The black contours in a and b are the climatic core position of the ACC (1991–2020). The blue and purple contours in a, b and c are the trends circumpolar contours for austral winter in 1960–1985 (a) and 1986–2021 (b). The contours in d–f and g–i are the same as a–c but for ocean current and wind stress vorticity.

that all three fields reflect the interdecadal shift of the meridional meanders of the ACC that occurred during the two periods. Therefore, how is this decadal shift related to the variation in MLD in the ACC region? Previous studies have shown that mixing along isopycnals is suppressed by one to two orders of magnitude in the core of the ACC jets, where the flow is sufficiently strong to carry tracers downstream before eddies have a change to mix cross-stream (Ferrari and Nikurashin, 2010). On the other hand, widespread and strong shears exist on the flanks of the ACC, which support the generation and development of mixing processes (Rintoul, 2018). The flow axis of the ACC tended to drift toward the equator in the SP sector; therefore, the original inhibited mixing activities began to develop under the newly formed shear after the flow core moved away (approximately 54°–65°S in Fig. 5d), resulting in a deepening trend for MLD in the ACC region toward the Antarctic. In the SI sector, there was a drifting trend toward the Antarctic for the flow axis of the ACC, and the position of the original core turned into the flank of the ACC, fa-

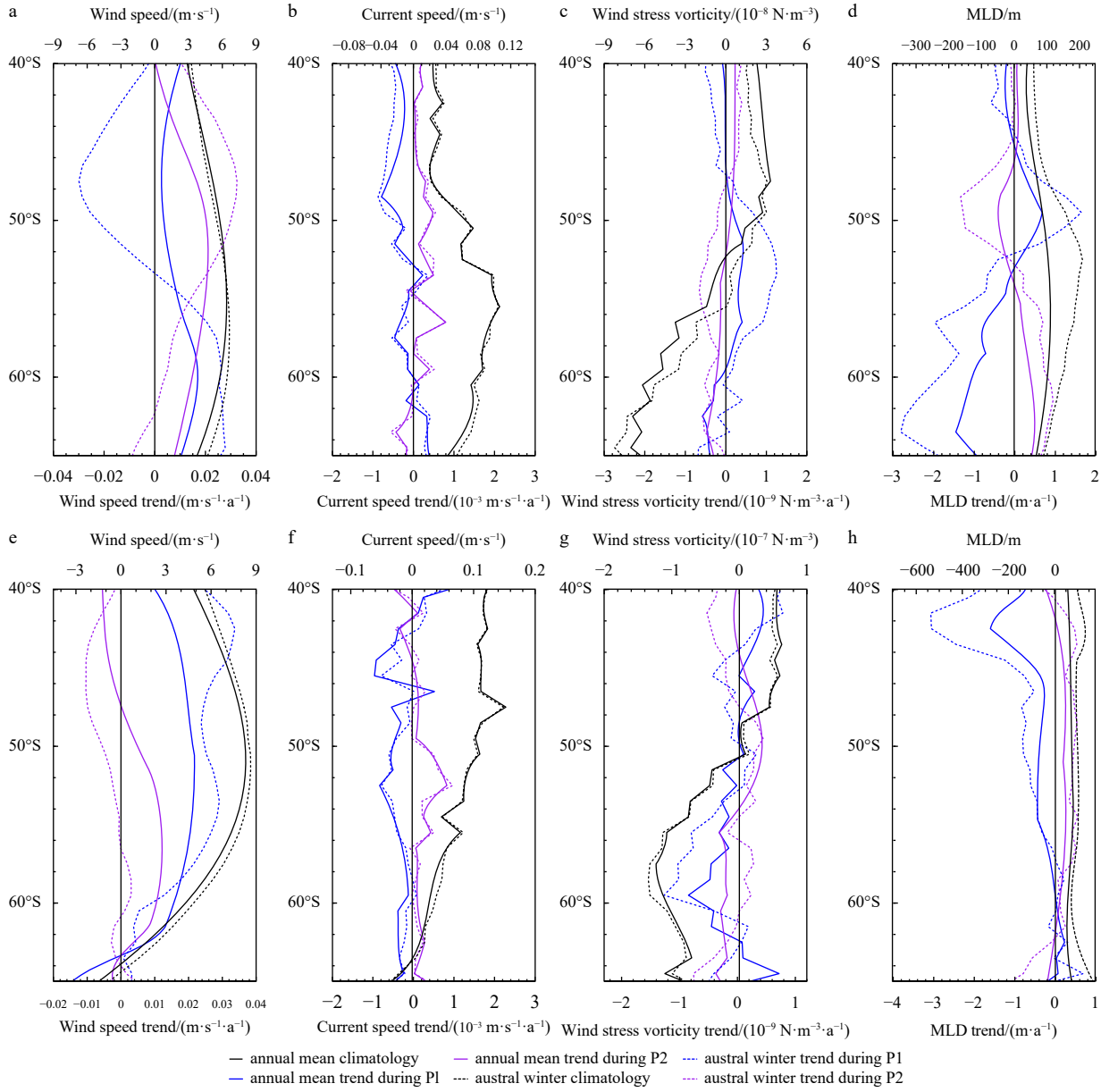

Fig. 5. The annual mean (solid lines) and winter (dashed lines) zonal averaged profiles for climatology (black lines) and trends (blue and purple lines) of surface wind speed (a), ocean current speed (b), wind stress vorticity (c) and MLD (d) from 40°S to 65°S in the SP sector (70°W–180°). e, f, g and h are the same as a, b, c and d but for the SI sector (0°–90°E). The climatological values are based on the period of 1991–2020. The blue and purple lines are the corresponding zonal mean trends in the periods 1960–1985 (P1 in the legend) and 1986–2021 (P2 in the legend), respectively.

voring mixing processes there (approximately 42°–56°S in Fig. 5h). As a result, the MLD tended to deepen on the equatorward side of the ACC flow axis. All these findings are in good agreement with the conclusions shown in Figs 2c and i.

To further investigate the influence of flow axis variations on the MLD trend changes, two key regions (green boxes in Fig. 2i) with pronounced flow axis oscillation are selected: the southwestern region of Drake Strait (60°–68°S, 76°–150°W, K1 hereafter) and the central South Indian Ocean region (40°–50°S, 50°–90°E, K2 hereafter). It is the trend variation rather than interannual change that the study focuses on. Therefore, an 11-year running mean are performed to the time series. The standardized time series are shown in Fig. 6. The MLD and related variable changes in the K1 region for annual mean results (Fig. 6a) shows the opposite phases between MLD and the three dynamic variables, along with the shallowing followed by deepening trends of MLD, the wind speed, ocean current and wind stress vorticity gradient all display increasing trends followed by decreasing trends. Their correlation coefficients with MLD are –0.28, –0.60, and –0.56, respectively. This indicates that the deviation of flow axis from K1 region are favorably to MLD deepening here. Similar negative relationship is derived from the results in K2 region (Fig. 6b), where the negative correlations of wind speed, ocean current, and wind stress curl gradients with MLD are –0.79, –0.30, and –0.42, respectively. The winter mean results are shown in Figs 6c and d. The inverse changes of these time series well reveal the inhibition effect of the flow axis on MLD deepening, as well as the promotion effect of the flow axis depar-

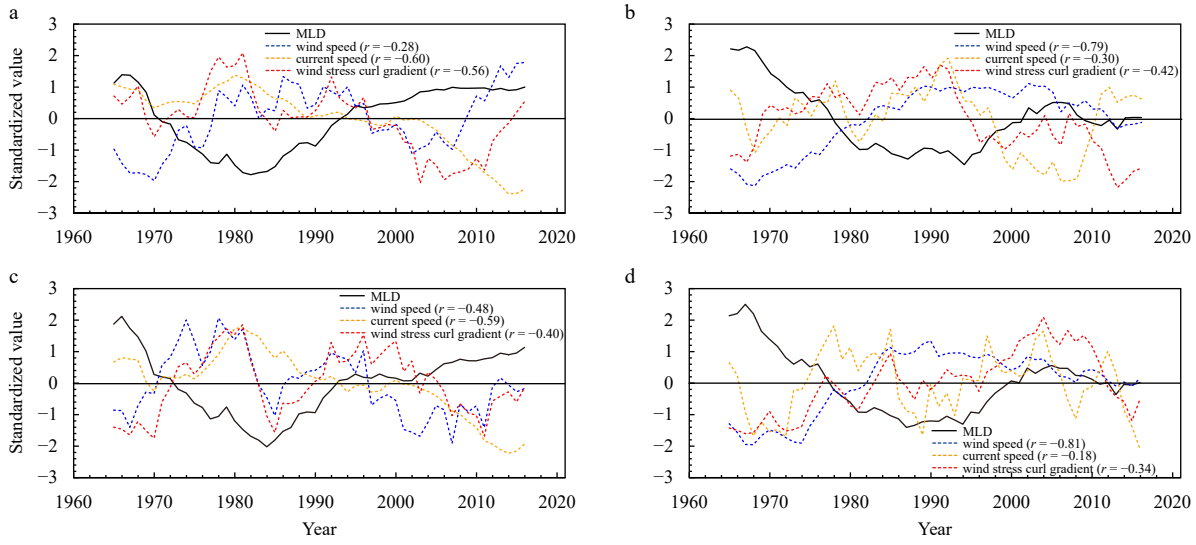

Fig. 6. The annual mean and winter standardized time series of MLD (black solid line), wind speed (blue dashed line), ocean current speed (orange dashed line) and wind stress curl meridional gradient (red dashed line) in K1 (60°–68°S, 76°–150°W) (a) and K2 (40°–50°S, 50°–90°E) (b) regions. The correlations between MLD and the corresponding variables are given in the following brackets. c and d are the same as a and b, but for winter mean.

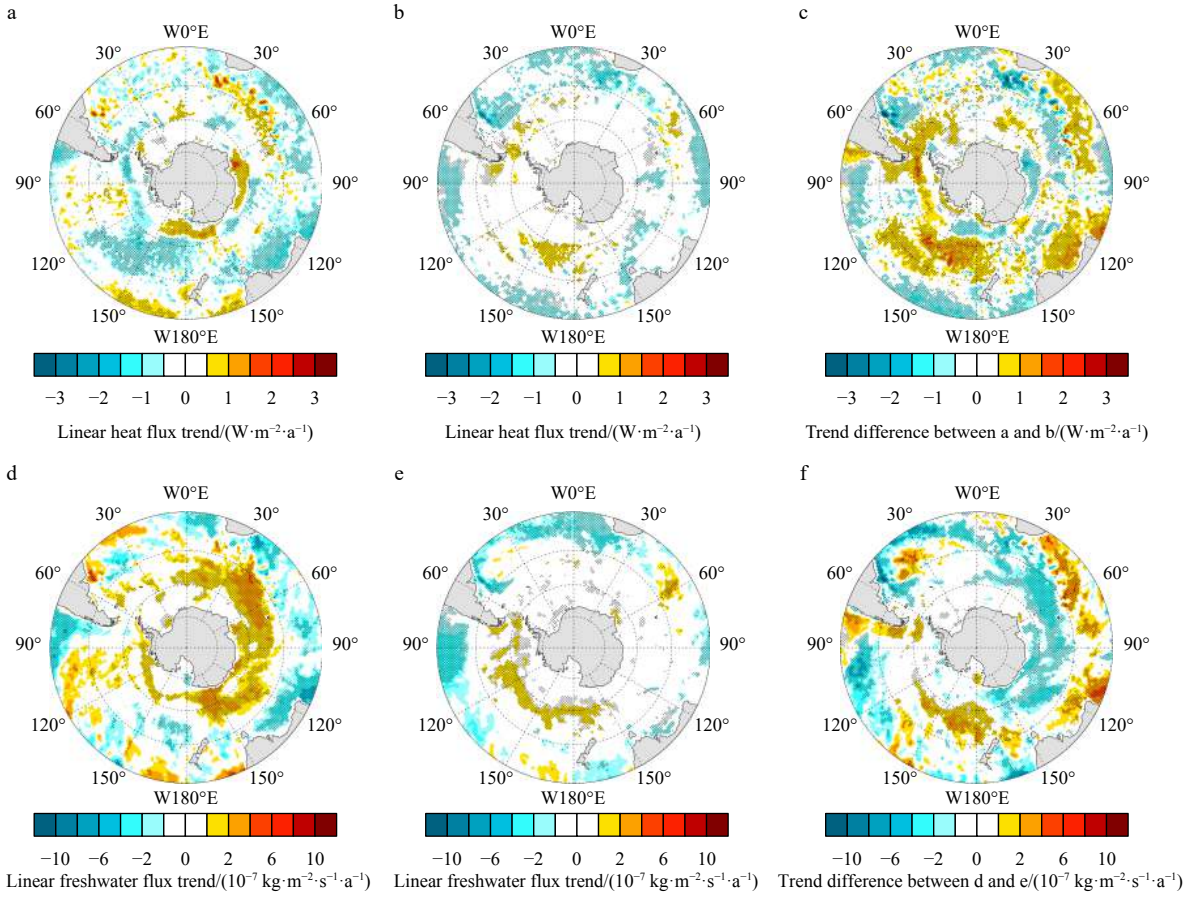

Fig. 7. Spatial patterns of the annual mean linear heat flux trend in the ACC region for 1960–1985 (a) and 1986–2021 (b). c is the difference between a and b. d, e and f are the same as a, b and c but for freshwater. The convention is that downward fluxes are positive.

ture on MLD development.

The contributions of the heat flux and freshwater in the ACC region were also checked (Fig. 7). In climatology, the ocean loses heat to the atmosphere in the ACC region. In the former period, there were significant decreasing trends for the heat flux in the central Pacific sector and the areas south to Australia. This means that the ocean loses more heat in these areas, which can contribute to the weakening stratification and MLD deepening (Fig. 7a).

In addition, around the northern region of the Wilkes Land and the Ross Sea, there were small ranges of positive heat flux trends. In the latter period, these trends were both diminished. Compared with the MLD trend shift (Fig. 2c), these significant deepening trend regions could not correspond well with the variations in heat flux, where the trend shifts were almost positive, representing a heating effect that was not conducive to the MLD deepening here. This indicates that the heat flux trend variation is not the dominant factor driving the deepening MLD trends in the ACC region, which is consistent with the conclusion that the upper ocean stability is almost established by the vertical salinity gradient in the high latitudes due to the cold climate conditions there (Sallée et al., 2021). The freshwater flux in 1960–1985 mainly showed increasing trends in the high latitudes around Antarctica, while in 1986–2021, the increasing trends almost disappeared (Figs 7d and e). The saltier trend shift occupied most areas in the ACC region, and a freshening trend shift emerged in the western Pacific and a zonal band between 30°–45°S in the Indian Ocean (Fig. 7f). Compared with the MLD trends in Fig. 2c, the area north to Victoria Land and Wilkes Land (45°–60°S, 120°E–180°) with saltier trend shifts at maximum magnitudes of -7.08×10^{-7} kg/(m^2·s·a) and -4.14×10^{-7} kg/(m^2·s·a) are in good agreement with the deepening MLD there, where the deepening trend of MLD cannot be explained by the dynamic fields due to the absence of axis shift of the ACC.

In summary, the interdecadal shift in MLD trends in the ACC region could be primarily attributed to the meridional shift in the flow axis of the ACC between the two periods, especially for the deepening trends in the SI and SP sectors mentioned above. Meanwhile, the saltier trends of freshwater flux north to Victoria Land and Wilkes Land match well with the strengthening mixing processes there.

4 Summary and conclusions

Over the past decades during 1960–2021, the annual mean and winter MLD in the ACC region experienced an obvious trend shift around the mid-1980s. The MLD shallowed at a rate of –0.18 m/a during 1960–1985 and maintained a period with almost no trend in 1986–2021. This indicates that the MLD in this region has not become continuously shallower as expected under the background of global warming but has stopped deepening since the mid-1980s. The deepening trend shift of MLD trends in the ACC region was mainly distributed in the western areas in the Drake Passage of the SP sector, the areas north to Victoria Land and Wilkes Land, and the central parts of the SI sector.

However, unlike the well understanding of global mixed-layer shoaling in a warming climate, unexpected MLD trend shift needs more explanation. By investigating wind speed, current ocean, wind stress vorticity, net heat flux and freshwater flux, attribution analysis of the evolution mechanism of the MLD trends in the ACC region was conducted to explore the drivers of the MLD trend change. A common feature of an interdecadal drift in the flow axis of the ACC is revealed by all three dynamic fields. The SI sector experienced a polarward compression of the ACC flow axis in the meridional direction, while the SP sector experienced an expansion to the equatorial direction. Therefore, the newly formed shear due to the meridional shift of the ACC flow axis creates favorable conditions for the generation and development of the mixing processes there, leading to MLD deepening there. In addition, the saltier trends of the freshwater flux in the area north to Victoria Land and Wilkes Land may be responsible for the deepening MLD, where the interdecadal shift of the flow axis of the ACC was inapparent there. The variation trend for heat flux in the ACC region could not explain the corresponding trend change in MLD, which may not be the dominant contributor for the deepening trends here.

Considering the significant role of the Southern Ocean in a continuing warming world, there will be broad and profound changes in the ACC region in the future. The question of whether the variation trend of MLD will deepen or reverse to shoal requires continuous attention. The contribution analysis for trend change of the MLD requires not only exploration of the thermohaline conditions but also comprehensive investigation of the dynamic fields. Further studies are needed to explore how the shift of the ACC axis, the atmospheric circulation pattern and the thermohaline forcing affect the trends of MLD in the ACC region in different projections.

References

An Yuzhu, Zhang Ren, Wang Huizan, et al. 2012. Study on calculation and spatio-temporal variations of global ocean mixed layer depth. Chinese Journal of Geophysics (in Chinese), 55(7): 2249–2258

Barkan R, Winters K B, McWilliams J C. 2017. Stimulated imbalance and the enhancement of eddy kinetic energy dissipation by internal waves. Journal of Physical Oceanography, 47(1): 181–198, doi: 10.1175/JPO-D-16-0117.1

Böning C W, Dispert A, Visbeck M, et al. 2008. The response of the Antarctic Circumpolar Current to recent climate change. Nature Geoscience, 1(12): 864–869, doi: 10.1038/ngeo362

Buckingham C E, Lucas N S, Belcher S E, et al. 2019. The contribution of surface and submesoscale processes to turbulence in the open ocean surface boundary layer. Journal of Advances in Modeling Earth Systems, 11(12): 4066–4094, doi: 10.1029/2019MS001801

Cheng Lijing, Trenberth K, Fasullo J, et al. 2017. Improved estimates of ocean heat content from 1960 to 2015. Science Advances, 3(3): e1601545, doi: 10.1126/sciadv.1601545

de Boyer Montégut C, Gurvan M, Fischer A S, et al. 2004. Mixed layer depth over the global ocean: an examination of profile data and a profile-based climatology. Journal of Geophysical Research: Oceans, 109(C12): C12003, doi: 10.1029/2004JC002378

Deser C, Alexander M A, Timlin M S. 1996. Upper-ocean thermal variations in the North Pacific during 1970–1991. Journal of Climate, 9(8): 1840–1855, doi: 10.1175/1520-0442(1996)009<1840:UOTVIT>2.0.CO;2

Downes S M, Bindoff N L, Rintoul S R. 2009. Impacts of climate change on the subduction of mode and intermediate water masses in the Southern Ocean. Journal of Climate, 22(12): 3289–3302, doi: 10.1175/2008JCLI2653.1

Downes S M, Bindoff N L, Rintoul S R. 2010. Changes in the subduction of Southern Ocean water masses at the end of the Twenty-First century in eight IPCC models. Journal of Climate, 23(24): 6526–6541, doi: 10.1175/2010JCLI3620.1

Feng Licheng, Zhang Ronghua, Yu Bo, et al. 2020. Roles of wind stress and subsurface cold water in the second-year cooling of the 2017/18 La Niña event. Advances in Atmospheric Sciences, 37(8): 847–860, doi: 10.1007/s00376-020-0028-4

Ferrari R, Nikurashin M. 2010. Suppression of eddy diffusivity across jets in the Southern Ocean. Journal of Physical Oceanography, 40(7): 1501–1519, doi: 10.1175/2010JPO4278.1

Giunta V, Ward B. 2022. Ocean mixed layer depth from dissipation. Journal of Geophysical Research: Oceans, 127(4): e2021JC017904, doi: 10.1029/2021JC017904

Hersbach H, Bell B, Berrisford P, et al. 2020. The ERA5 global reanalysis. Quarterly Journal of the Royal Meteorological Society, 146(730): 1999–2049, doi: 10.1002/qj.3803

Huang Chuanjiang, Qiao Fangli, Dai Dejun. 2014. Evaluating CMIP5 simulations of mixed layer depth during summer. Journal of Geophysical Research: Oceans, 119(4): 2568–2582, doi: 10.1002/2013JC009535

Huang Chuanjiang, Qiao Fangli, Shu Qi, et al. 2012. Evaluating austral summer mixed-layer response to surface wave-induced mixing in the Southern Ocean. Journal of Geophysical Research: Oceans, 117(C11): C00J18, doi: 10.1029/2012JC007892

Huang Ruixin, Qiu Bo. 1998. The structure of the wind-driven circulation in the subtropical South Pacific Ocean. Journal of Physical Oceanography, 28(6): 1173–1186, doi: 10.1175/1520-0485(1998)028<1173:TSOTWD>2.0.CO;2

Li Guancheng, Cheng Lijing, Zhu Jiang, et al. 2020. Increasing ocean stratification over the past half-century. Nature Climate Change, 10(12): 1116–1123, doi: 10.1038/s41558-020-00918-2

Liu Shan, Jing Xueyi, Chen Xingrong, et al. 2023. An assessment of the subduction rate in the CMIP6 historical experiment. Acta Oceanologica Sinica, 42(1): 44–60, doi: 10.1007/s13131-022-2108-z

Liu Chengyan, Wu Lixin. 2012. An intensification trend of South Pacific Mode Water subduction rates over the 20th century. Journal of Geophysical Research: Oceans, 117(C7): C07009, doi: 10.1029/2011JC007755

Munday D R, Johnson H L, Marshall D P. 2013. Eddy saturation of equilibrated circumpolar currents. Journal of Physical Oceanography, 43(3): 507–532, doi: 10.1175/JPO-D-12-095.1

Ohno Y, Iwasaka N, Kobashi F, et al. 2009. Mixed layer depth climatology of the North Pacific based on Argo observations. Journal of Oceanography, 65(1): 1–16, doi: 10.1007/s10872-009-0001-4

Rintoul S R. 2018. The global influence of localized dynamics in the Southern Ocean. Nature, 558(7709): 209–218, doi: 10.1038/s41586-018-0182-3

Russell J L, Dixon K W, Gnanadesikan A, et al. 2006. The Southern Hemisphere westerlies in a warming world: propping open the door to the deep ocean. Journal of Climate, 19(24): 6382–6390, doi: 10.1175/JCLI3984.1

Sallée J B, Pellichero V, Akhoudas C, et al. 2021. Summertime increases in upper-ocean stratification and mixed-layer depth. Nature, 591(7851): 592–598, doi: 10.1038/s41586-021-03303-x

Sallée J B, Shuckburgh E, Bruneau N, et al. 2013. Assessment of Southern Ocean mixed-layer depths in CMIP5 models: historical bias and forcing response. Journal of Geophysical Research: Oceans, 118(4): 1845–1862, doi: 10.1002/jgrc.20157

Sallée J B, Speer K G, Rintoul S R. 2010. Zonally asymmetric response of the Southern Ocean mixed-layer depth to the Southern Annular Mode. Nature Geoscience, 3(4): 273–279, doi: 10.1038/ngeo812

Shi Jiarui, Talley L D, Xie Shangping, et al. 2021. Ocean warming and accelerating Southern Ocean zonal flow. Nature Climate Chang, 11: 1090–1097, doi: 10.1038/s41558-021-01212-5

Somavilla R, González-Pola C, Fernández-Diaz J. 2017. The warmer the ocean surface, the shallower the mixed layer. How much of this is true?. Journal of Geophysical Research: Oceans, 122(9): 7698–7716, doi: 10.1002/2017JC013125

Stewart A L. 2021. Warming spins up the Southern Ocean. Nature Climate Change, 11(12): 1022–1024, doi: 10.1038/s41558-021-01227-y

Toggweiler J R, Russell J. 2008. Ocean circulation in a warming climate. Nature, 451(7176): 286–288, doi: 10.1038/nature06590

Yamaguchi R, Suga T. 2019. Trend and variability in global upper-ocean stratification since the 1960s. Journal of Geophysical Research: Oceans, 124(12): 8933–8948, doi: 10.1029/2019JC015439

Yang Xiaoyi, Huang Ruixin, Wang Dongxiao. 2007. Decadal changes of wind stress over the Southern Ocean associated with Antarctic ozone depletion. Journal of Climate, 20(14): 3395–3410, doi: 10.1175/JCLI4195.1

Zhang Yutong, Xu Haiming, Qiao Fangli, et al. 2018. Seasonal variation of the global mixed layer depth: comparison between Argo data and FIO-ESM. Frontiers of Earth Science, 12(1): 24–36, doi: 10.1007/s11707-017-0631-6